Time-Dependent Density Functional Study of the Electronic Excited States of Polycyclic Aromatic Hydrocarbon Radical Ions

So Hirata*

William R. Wiley Environmental Molecular Sciences Laboratory, Pacific Northwest National Laboratory, P.O. Box 999, Richland, Washington 99352

Martin Head-Gordon

Department of Chemistry, University of California, Chemical Sciences Division, Lawrence Berkeley National Laboratory, Berkeley, California 94720

Jan Szczepanski and Martin Vala

Department of Chemistry and Center for Chemical Physics, University of Florida, Gainesville, Florida 32611-7200

Received: February 11, 2003

A uniform, comprehensive theoretical interpretation of spectroscopic data is presented for 51 radical ion species of polycyclic aromatic hydrocarbons (PAHs) with the aid of (Tamm−Dancoff) time-dependent density functional theory (TDDFT). TDDFT is capable of predicting the transition energies to the low-lying excited states of PAH ions with quantitative accuracy (the standard deviation from experimental results being less than 0.3 eV) and their intensity patterns qualitatively correctly. The accuracy is hardly affected by the sizes of PAH ions (azulene through dinaphthocoronene), the types of transitions (Koopmans or satellite transitions), the types of orbitals involved ($\pi^* \leftarrow \pi$, $\pi^* \leftarrow \sigma$, or $\sigma^* \leftarrow \pi$ transitions), the types of ions (cations or anions), or other geometrical or electronic perturbations (nonplanarity, sp^3 carbons, or heterocyclic or nonbenzenoid rings).

1. Introduction

Polycyclic aromatic hydrocarbons (PAHs) constitute a large class of conjugated π-electron systems that are key molecular species in many branches of chemistry, such as, interstellar, combustion, environmental, and materials chemistry. These species are detected in meteorites, are strong candidates for the carriers of interstellar infrared emission features and diffuse interstellar visible absorption bands, and are thought to be a major carbon reservoir in the interstellar medium.[1−7] They are also primary intermediate species that form in combustion processes[8−10] and are the most ubiquitous environmental contaminants from natural and man-made sources with varied mutagenic and carcinogenic activities.[11−13] It has been proposed that PAHs are the precursors of flame-produced soot[9] and fullerenes.[14−16]

Radical ions of PAHs play a crucial role in these processes. They predominate in combustion systems because PAH growth (as well as the soot and fullerene formation) in hydrocarbon combustion likely occurs by sequential additions of a small acetylenic species with PAH radicals.[16] The mutagenic and carcinogenic activities of PAHs may be due to free radical reactions and can be correlated with their ionization potentials.[13] In the interstellar medium, a large fraction of PAHs are expected to be ionized by the strong UV radiation present in the environment. Ionized PAHs absorb lower-energy photons than their neutral counterparts, and astrophysical observations appear to favor the spectral features of the former over those of the latter.[17−20] Recently, the infrared emission from the radical cation of a PAH has been observed in a laboratory experiment.[21]

A wealth of spectroscopic data for PAH radical ions has been amassed. Electronic absorption spectra of a large number of radical cations and anions[22−49] and high-resolution photoelectron spectra of neutral species[50−55] have been measured with the matrix isolation technique or in the gas phase. Theoretical interpretation of these comprehensive spectroscopic data sets, however, has significantly lagged behind the experimental efforts. Although some accurate multireference configuration interaction methods,[56] multireference perturbation methods,[44,57,58] and many-body Green's function methods[59,60] have been applied to small PAH radical ions, the majority of the calculations of PAH radical ions has been limited to those based either on Koopmans' theorem or on semiempirical methods. This is primarily due to the difficulty in describing the excited-state wave functions of open-shell systems theoretically and the large sizes of important PAH radical ions, which become a bottleneck for theoretical methods of which the computational costs scale steeply with system size.

We have recently shown that time-dependent density functional theory (TDDFT)[61−66] was a tool particularly well-suited for the interpretation of the electronic absorption spectra of PAH radical ions and the photoelectron spectra of neutral PAHs[67] (see also refs 45 and 68). The computational cost of TDDFT calculations is comparable to that of a Hartree−Fock-based single excitation theory, for example, configuration interaction singles (CIS) or time-dependent Hartree−Fock (TDHF) method.

* To whom correspondence should be addressed. Electronic mail address: so.hirata@pnl.gov.

10.1021/jp0301913 CCC: $25.00
Published on Web 05/23/2003

Moreover, it preserves the orbital pictures that chemists are accustomed to use in discussing spectral properties. TDDFT maintains a uniform accuracy for open-shell and closed-shell systems.[69] This is in contrast to CIS and TDHF, which tend to break down for open-shell wave functions.[70] Remarkably, for the PAH radical cations of small to intermediate sizes that we studied previously, the excitation energies obtained from TDDFT were typically within a few tenths of an electronvolt of the experimental data.[67] Unlike multireference methods in which a selected group of orbitals (an active space, which is typically dominated by π-orbitals for conjugated π-electron systems) is treated differently from the rest, TDDFT provides an unbiased description of both the $\pi^* \leftarrow \pi$ and $\pi^* \leftarrow \sigma$ ($\sigma^* \leftarrow \pi$) excitation processes.[67]

In this article, we present a theoretical interpretation of comprehensive spectroscopic data of PAHs on the basis of TDDFT calculations. The electronic absorption spectra of radical cations and the photoelectron spectra of neutral species are compared with the calculated vertical excitation energies of radical cations for a list of PAHs consisting of 25 catacondensed, 15 peri-condensed, 8 nonbenzenoid or noncondensed aromatic, and 3 heterocyclic hydrocarbons (51 species in total). The electronic absorption spectra of radical anions are also theoretically analyzed for 7 PAH species. Apart from the uniform theoretical interpretation of the experimental data that it offers, the present study addresses the following. (1) *The σ ionization states*. The σ ionization manifolds mask any detailed feature of the photoelectron spectra, making it difficult to extract information about σ ionized states or higher-lying π ionized states experimentally. (2) *The differences and similarities in electronic absorption spectra between the cationic and the anionic forms of PAHs*. The cation and anion of an alternant hydrocarbon often give rise to almost identical electronic absorption spectra, although there are nonsystematic small shifts in the absorption band positions, the origin of which is not known precisely. (3) *Satellite (also known as shake-up or non-Koopmans) photoelectron peaks*. Satellite peaks are second- and higher-order electron ionization transitions and hence are completely missing in Koopmans' approximations. In fact, in some ionization theories, such as many-body Green's function theory, satellite peaks are treated differently from Koopmans transitions. We expect that TDDFT, which treats both Koopmans and two-electron-type satellite ionization transitions in the same fashion as one-electron excitation transitions in the cationic species, will provide a well-balanced description of the photoelectron peaks of both types. (4) *The nonplanarity or heteronuclear effects on the photoelectron and electronic absorption spectra of PAHs*. TDDFT treats σ and π orbitals, sp^2 and sp^3 carbon atoms, and carbon and other heteroatoms on an equal footing. The question is whether TDDFT can reproduce subtle spectral changes that arise from such structural and electronic perturbations.

2. Calculations

We optimized the geometries of the neutral PAHs by density functional theory (DFT) by using the Becke3−Lee−Yang−Parr (B3LYP) hybrid functional with the 6-31G** basis set. The structures of the neutral PAHs studied in this work are drawn schematically in Figure 1. We assumed the planarity of carbon skeletons for all the PAHs with the exceptions of 3.4,5.6-dibenzophenanthrene (**8**) and biphenyl (**48**) for which nonplanar helical equilibrium structures were determined. The vertical excitation energies and oscillator strengths were computed by TDDFT or Tamm−Dancoff TDDFT[71] using the Becke−Lee−Yang−Parr (BLYP) functional with the 6-31G** basis set for the PAH radical cations and using the same exchange−correlation functional with the 6-31G++G** basis set for the PAH radical anions at the neutral geometries. In this study, we consistently used neutral geometries because high-resolution photoelectron spectra were chosen as the primary experimental data against which the calculated excitation energies were compared. The electronic absorption spectra of radicals were used to verify the assignments. Although the electronic absorptions of radical cations or anions occur at the equilibrium geometries of the respective radical ions, the tacit assumption that the effects of the structural differences between neutral and cationic or anionic forms are small is usually valid. Comparison of the calculated vertical excitation energies of cations and anions at their neutral geometries highlights the spectral differences that have an electronic origin. The Tamm−Dancoff approximation, which is algorithmically more robust than the full time-dependent linear response theory, was invoked when the latter failed to give converged excitation energies.

The DFT calculations for the geometry optimizations and the TDDFT calculations for the excitation energies were carried out with a development version of the NWChem quantum chemistry program[72] that supported both sequential and parallel executions. For details of the TDDFT algorithms and their implementation adopted in NWChem, see Hirata and Head-Gordon.[69]

3. Results and Discussion

The vertical excitation energies and oscillator strengths of the radical cations of PAH calculated by TDDFT are compiled in Tables 1−4. Table 5 summarizes the calculated vertical excitation energies and oscillator strengths of radical anions of a subset of the PAHs shown in Figure 1. Experimental photoelectron spectra in these tables come from Boschi, Clar, and Schmidt[53] and Ruščić et al.,[55] while the electronic absorption spectra come from Shida and Iwata,[22,30] Khan,[26,28,31] Vala and co-workers,[17,35,37,39,41,42,49] and Allamandola and co-workers.[38,40,43,45,46]

The spectral band assignments are made according to the following principles. The photoelectron spectra of neutral PAHs are characterized by sharp, well-separated peaks of approximately equal intensities below ca. 10 eV. They correspond to Koopmans (as opposed to satellite) π ionization peaks that have only small or no vibrational structure. In the higher energy region, broad structureless steplike peaks start to overlap these sharp features, and these are identified as the σ ionization manifold; the loss of an electron from a σ orbital tends to weaken a chemical bond significantly, resulting in a dense manifold of vibrational progressions that accompanies the ionization peak. The energy differences between the lowest-energy peak (first ionization potential) and the higher-energy peaks are equal to the vertical excitation energies of the radical cations. We assign the energy differences between the first ionization potential and the sharp π ionization peaks (in the order of increasing energy differences) to the calculated electron excitations to the lowest unoccupied molecular orbital (LUMO) (designated as π_0^*) of radical cations (Koopmans transitions) from occupied orbitals (designated as π_{-1}, σ_{-2}, etc.) (Figure 2a). Those excitations that do not involve transitions to the LUMO (parenthesized for distinction in the tables) (Figure 2b,c) correspond to satellite peaks in photoelectron spectra, which will be virtually invisible in the photoelectron spectra. They may, however, be associated with intense electronic absorption bands of the corresponding radical cation. We assign the energy

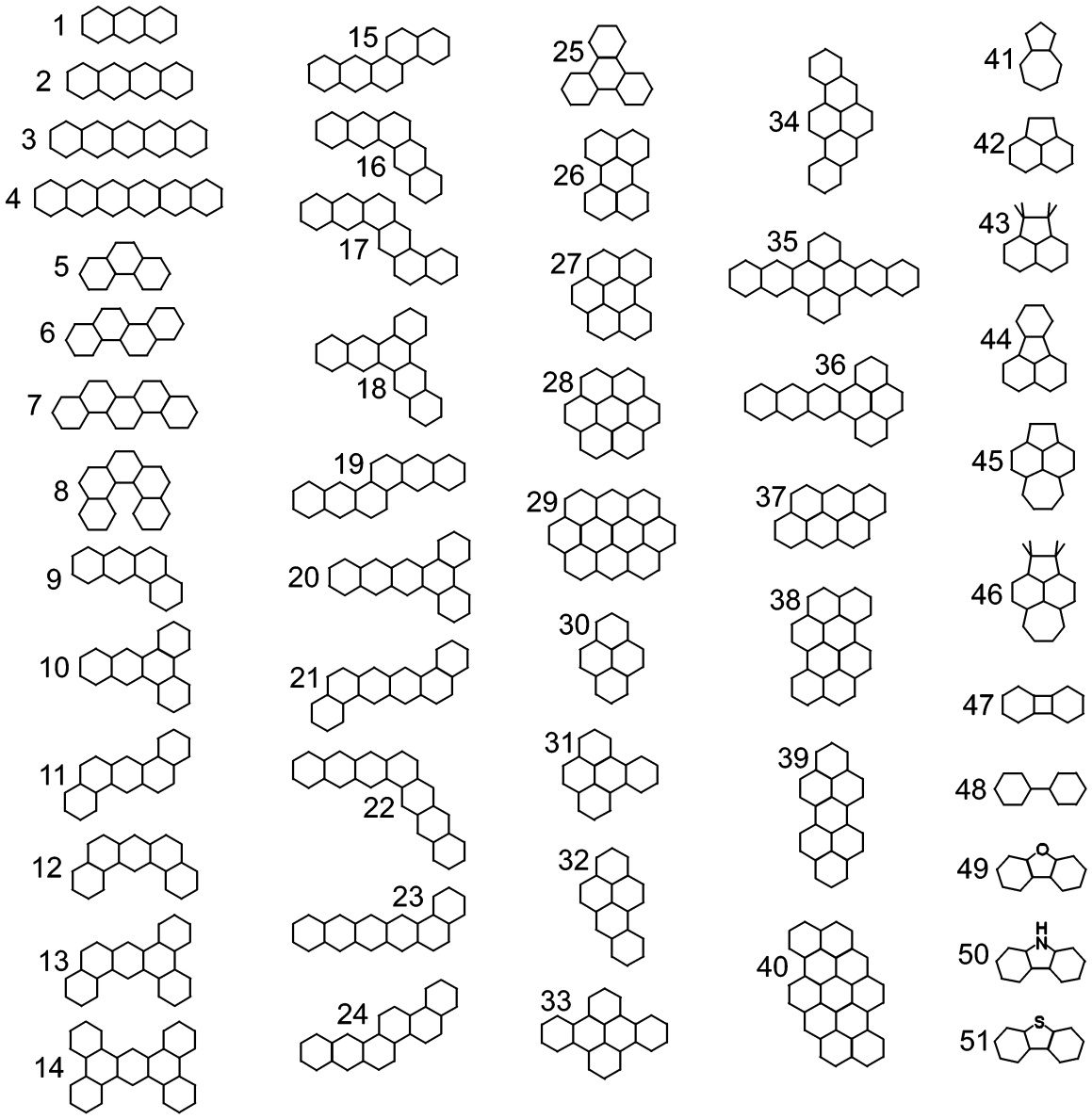

Figure 1. Structures of polycyclic aromatic hydrocarbons.

difference between the first ionization peak and the onset of the dense σ ionization manifolds (indicated by asterisks in the experimental data) to the lowest $\pi^* \leftarrow \sigma$ excitations that involve the LUMO.

Once the measured photoelectron peaks of a neutral PAH were assigned to the calculated data, we compared the calculated vertical excitation energies and oscillator strengths with the observed electronic absorption bands of the radical cation. Major electronic absorption bands were assigned to those excitations with significant oscillator strengths. They may or may not correspond to satellite ionization peaks, and, in this sense, photoelectron spectroscopy for neutral species and electronic absorption spectroscopy for cations are complementary techniques. For the radical anions of PAHs, prominent electronic absorption bands are assigned to the intense electronic excitations predicted by TDDFT.

The overall agreement between the theory and experiment is excellent for this selected but fairly large group of PAHs. The mean square deviations for all of the assigned photoelectron and electronic absorption bands are 0.26, 0.24, 0.19, 0.31, and 0.17 eV for Tables 1−5, respectively. This degree of agreement is comparable and sometimes even better than that expected from multireference perturbation theory, which requires far greater computational costs and careful selection of active space.

The calculated position of the lowest-lying $\pi^* \leftarrow \sigma$ transitions correlate well with the onsets of dense σ ionization manifolds determined from photoelectron spectra. The mean absolute deviation of the calculated onset of σ ionization manifolds from the experimental data is 0.42 eV, which is only slightly greater than the overall mean error. This is remarkable because these $\pi^* \leftarrow \sigma$ transitions are often completely missing in the results of active-space-based methods. However, the deviations of the TDDFT-calculated positions of the lowest-lying $\pi^* \leftarrow \sigma$ transitions from the experimental ionization manifold onsets[53] seem large and systematic compared to the smaller analogous deviations for the $\pi^* \leftarrow \pi$ transitions. This might be the consequence of an intensity redistribution into the vibronic transitions that manifest on the higher energy side of the $\pi^* \leftarrow \sigma$ transitions. This would make it appear that the σ transition onset lies at a higher energy than it actually does. For sizable PAH radical cations, such as 1.2,3.4,5.6,7.8-tetrabenzanthracene (**14**), pyreno-(1.3:10′.2′)-pyrene (**38**), and dinaphtho-(2′.8′:2.4);(1″.7″:10.8)-coronene (**40**), the differences between the calculated and experimental results seem uncharacteristically

TABLE 1: Vertical Excitation Energies (eV) and Oscillator Strengths of Cata-Condensed Aromatic Hydrocarbon Radical Cations

	calculation		experiment			calculation		experiment	
state (transition)	excitation energy[b]	oscillator strength	PE[c]	electronic absorption[d]	state (transition)	excitation energy[b]	oscillator strength	PE[c]	electronic absorption[d]
				(**1**) Anthracene (D_{2h}, b_{2g})					
b_{3g} ($\pi_0^* \leftarrow \pi_{-1}$)	1.25	*l*	1.10		b_{2g} ($\pi_0^* \leftarrow \pi_{-3}$)	2.73	*l*	2.79	
a_u ($\pi_0^* \leftarrow \pi_{-2}$)	1.81	0.086	1.76	1.71, 1.72[e]	b_{1u} ($\pi_0^* \leftarrow \pi_{-4}$)	2.90	0.046	2.93	2.83, 2.90[e]
b_{1u} ($\pi_1^* \leftarrow \pi_0$)	(2.37)	0.000		2.02[e]	a_g ($\pi_0^* \leftarrow \sigma_{-5}$)	3.08	*l*	3.3*	
				(**2**) Tetracene (D_{2h}, a_u)					
b_{1u} ($\pi_0^* \leftarrow \pi_{-2}$)	1.53	*l*	1.40		b_{1u} ($\pi_1^* \leftarrow \pi_{-1}$)	(3.02)	*l*		
b_{2g} ($\pi_0^* \leftarrow \pi_{-1}$)	1.58	0.133	1.59	1.43, 1.43,[f] 1.43[g]	b_{2g} ($\pi_0^* \leftarrow \pi_{-5}$)	3.16	0.003	3.22	
b_{3g} ($\pi_1^* \leftarrow \pi_0$)	(1.77)	0.007		1.65, 1.66[f]	b_{2g} ($\pi_3^* \leftarrow \pi_0$)	(3.36)	0.032		3.14, 3.16[f]
a_u ($\pi_0^* \leftarrow \pi_{-3}$)	2.44	*l*	2.56		a_g ($\pi_0^* \leftarrow \sigma_{-6}$)	3.37	*l*	3.7*	
b_{3g} ($\pi_0^* \leftarrow \pi_{-4}$)	2.69	0.031	2.71						
				(**3**) Pentacene (D_{2h}, b_{2g})					
b_{1u} ($\pi_1^* \leftarrow \pi_0$)	(1.30)	0.007		1.26[i]	b_{3g} ($\pi_2^* \leftarrow \pi_0$)	(2.78)	*l*		
a_u ($\pi_0^* \leftarrow \pi_{-1}$)	1.39	0.185	1.29	1.30,[h] 1.30[i]	a_u ($\pi_0^* \leftarrow \pi_{-5}$)	2.88	0.007	3.14	
b_{3g} ($\pi_0^* \leftarrow \pi_{-2}$)	1.72	*l*	1.66		a_u ($\pi_3^* \leftarrow \pi_0$)	(3.08)	0.066		2.91,[h] 2.92[i]
b_{2g} ($\pi_0^* \leftarrow \pi_{-3}$)	2.17	*l*	2.35		b_{2g} ($\pi_0^* \leftarrow \pi_{-6}$)	3.44	*l*	3.59	
b_{3g} ($\pi_1^* \leftarrow \pi_{-1}$)	(2.34)	*l*			a_g ($\pi_0^* \leftarrow \sigma_{-7}$)	3.56	*l*	3.8*	
b_{1u} ($\pi_0^* \leftarrow \pi_{-4}$)	2.57	0.021	2.75						
				(**4**) Hexacene (D_{2h}, a_u)					
b_{3g} ($\pi_1^* \leftarrow \pi_0$)	(0.95)	0.006			b_{2g} ($\pi_0^* \leftarrow \pi_{-5}$)	2.62	0.009	2.92	
b_{2g} ($\pi_0^* \leftarrow \pi_{-1}$)	1.24	0.243	1.11		b_{3g} ($\pi_2^* \leftarrow \pi_{-1}$)	(2.78)	0.006		
b_{1u} ($\pi_1^* \leftarrow \pi_{-1}$)	(1.82)	*l*			b_{2g} ($\pi_3^* \leftarrow \pi_0$)	(2.87)	0.127		
b_{1u} ($\pi_0^* \leftarrow \pi_{-3}$)	1.86	*l*	1.70		b_{3g} ($\pi_4^* \leftarrow \pi_0$)	(3.11)	0.024		
a_u ($\pi_0^* \leftarrow \pi_{-2}$)	1.93	*l*	2.12		a_u ($\pi_0^* \leftarrow \pi_{-6}$)	3.19	*l*	3.51	
b_{1u} ($\pi_2^* \leftarrow \pi_0$)	(2.26)	*l*			b_{3g} ($\pi_4^* \leftarrow \pi_0$)	(3.35)	0.025		
b_{3g} ($\pi_0^* \leftarrow \pi_{-4}$)	2.51	0.009	2.92		a_u ($\pi_1^* \leftarrow \pi_{-4}$)	(3.41)	*l*		
				(**5**) Phenanthrene[a] (C_{2v}, b_2)					
a_2 ($\pi_0^* \leftarrow \pi_{-1}$)	0.31	0.002	0.29		b_1 ($\pi_0^* \leftarrow \sigma_{-5}$)	2.51	*l*	2.7*	
a_2 ($\pi_0^* \leftarrow \pi_{-2}$)	1.71	0.096	1.42	1.36, 1.38[j]	a_1 ($\pi_0^* \leftarrow \sigma_{-6}$)	2.74	0.000	2.73	
b_2 ($\pi_0^* \leftarrow \pi_{-3}$)	1.72	0.001	2.03	1.95[j]	b_2 ($\pi_0^* \leftarrow \pi_{-4}$)	2.77	0.036		2.56, 2.63[j]
				(**6**) Chrysene (C_{2h}, a_u)					
a_u ($\pi_0^* \leftarrow \pi_{-1}$)	0.50	*l*	0.50		a_g ($\pi_0^* \leftarrow \sigma_{-5}$)	2.60	0.000	3.0*	
b_g ($\pi_0^* \leftarrow \pi_{-2}$)	1.14	0.085	1.08	1.05	b_g ($\pi_0^* \leftarrow \pi_{-6}$)	2.78	0.014	2.92	2.58
b_g ($\pi_0^* \leftarrow \pi_{-3}$)	1.60	0.012	1.86	1.82	a_g ($\pi_0^* \leftarrow \sigma_{-7}$)	2.94	0.000		
a_u ($\pi_0^* \leftarrow \pi_{-4}$)	2.00	*l*	2.16		a_u ($\pi_0^* \leftarrow \pi_{-8}$)	3.06	*l*		
				(**7**) Picene[a] (C_{2v}, b_2)					
a_2 ($\pi_0^* \leftarrow \pi_{-1}$)	0.33	0.006	0.13		b_2 ($\pi_0^* \leftarrow \pi_{-4}$)	1.73	0.004	1.74	
b_2 ($\pi_0^* \leftarrow \pi_{-3}$)	1.16	0.001	0.82	0.92	a_2 ($\pi_0^* \leftarrow \pi_{-5}$)	2.15	0.002	2.38	2.54
a_2 ($\pi_0^* \leftarrow \pi_{-2}$)	1.23	0.282	1.52		b_1 ($\pi_0^* \leftarrow \sigma_{-6}$)	2.51	*l*		
				(**8**) 3.4,5.6-Dibenzophenanthrene[a] (C_2, a)					
b ($0^* \leftarrow -1$)	0.16	0.000	0.23		a ($0^* \leftarrow -4$)	1.90	0.036	2.01	
b ($0^* \leftarrow -2$)	1.05	0.120	0.82		b ($0^* \leftarrow -5$)	1.95	0.001	2.30	
a ($0^* \leftarrow -3$)	1.14	0.001	1.34		b ($0^* \leftarrow -6$)	2.42	0.031	2.50	
				(**9**) Tetraphene (C_s, a″)					
a″ ($\pi_0^* \leftarrow \pi_{-1}$)	0.53	0.003	0.58	0.86	a″ ($\pi_0^* \leftarrow \pi_{-4}$)	2.31	0.016	2.48	2.19
a″ ($\pi_0^* \leftarrow \pi_{-2}$)	1.45	0.067	1.39	1.41	a″ ($\pi_1^* \leftarrow \pi_0$)	(2.60)	0.006		2.43
a″ ($\pi_0^* \leftarrow \pi_{-3}$)	1.68	0.032	1.92	1.91	a′ ($\pi_0^* \leftarrow \sigma_{-6}$)	2.82	0.000	3.2*	2.58
				(**10**) 1.2,3.4-Dibenzanthracene (C_{2v}, a_2)					
b_1 ($\pi_0^* \leftarrow \pi_{-1}$)	0.46	0.002	0.48		a_2 ($\pi_0^* \leftarrow \pi_{-6}$)	2.42	0.001	2.53	2.54[k]
a_2 ($\pi_0^* \leftarrow \pi_{-2}$)	0.60	0.012	0.86	0.98[k]	b_2 ($\pi_0^* \leftarrow \sigma_{-7}$)	2.68	0.000	3.2*	2.66[k]
a_2 ($\pi_0^* \leftarrow \pi_{-3}$)	1.59	0.097	1.72	1.69[k]	b_1 ($\pi_1^* \leftarrow \pi_0$)	(2.68)	0.011		3.09[k]
b_1 ($\pi_0^* \leftarrow \pi_{-4}$)	1.68	0.000	1.96	1.85[k]	a_1 ($\pi_0^* \leftarrow \sigma_{-8}$)	2.69	*l*		
b_1 ($\pi_0^* \leftarrow \pi_{-5}$)	2.03	0.044	2.53	2.38[k]					
				(**11**) 1.2,5.6-Dibenzanthracene (C_s, a″)					
a″ ($\pi_0^* \leftarrow \pi_{-1}$)	0.32	0.000	0.44		a′ ($\pi_0^* \leftarrow \sigma_{-7}$)	2.72	0.000		
a″ ($\pi_0^* \leftarrow \pi_{-2}$)	0.88	0.036	1.05	1.06[k]	a′ ($\pi_0^* \leftarrow \sigma_{-8}$)	2.97	0.000	3.35	
a″ ($\pi_0^* \leftarrow \pi_{-3}$)	1.41	0.098	1.64	1.64[k]	a′ ($\pi_0^* \leftarrow \sigma_{-9}$)	3.01	0.000		
a″ ($\pi_0^* \leftarrow \pi_{-4}$)	1.68	0.000	1.88		a′ ($\pi_0^* \leftarrow \sigma_{-11}$)	3.21	0.000	3.3*	
a″ ($\pi_0^* \leftarrow \pi_{-5}$)	2.32	0.000	2.66		a″ ($\pi_2^* \leftarrow \pi_0$)	(3.49)	0.194		3.25[k]
a″ ($\pi_0^* \leftarrow \pi_{-6}$)	2.52	0.020	2.66	2.41[k]					
				(**12**) 1.2,7.8-Dibenzanthracene[a] (C_{2v}, b_2)					
a_2 ($\pi_0^* \leftarrow \pi_{-1}$)	0.33	0.005	0.41		a_2 ($\pi_0^* \leftarrow \pi_{-5}$)	1.97	0.025	2.22	2.12
b_2 ($\pi_0^* \leftarrow \pi_{-2}$)	0.89	0.001	1.23	1.24	b_2 ($\pi_0^* \leftarrow \pi_{-4}$)	2.07	0.034	2.22	2.32
a_2 ($\pi_0^* \leftarrow \pi_{-3}$)	1.50	0.197	1.43	1.39	a_1 ($\pi_0^* \leftarrow \sigma_{-7}$)	2.72	0.000	3.0*	2.90

TABLE 1: Continued

	calculation		experiment			calculation		experiment	
state (transition)	excitation energy[b]	oscillator strength	PE[c]	electronic absorption[d]	state (transition)	excitation energy[b]	oscillator strength	PE[c]	electronic absorption[d]
(**13**) 1.2,3.4,5.6-Tribenzanthracene (C_s, a″)									
a″ ($\pi_0^* \leftarrow \pi_{-1}$)	0.20	0.000	0.15		a″ ($\pi_0^* \leftarrow \pi_{-5}$)	1.83	0.007	2.17	
a″ ($\pi_0^* \leftarrow \pi_{-2}$)	0.59	0.019	0.82		a″ ($\pi_0^* \leftarrow \pi_{-6}$)	2.01	0.039	2.41	
a″ ($\pi_0^* \leftarrow \pi_{-3}$)	0.88	0.012	1.26		a″ ($\pi_0^* \leftarrow \pi_{-7}$)	2.27	0.004	2.59	
a″ ($\pi_0^* \leftarrow \pi_{-4}$)	1.39	0.100	1.64		a′ ($\pi_0^* \leftarrow \sigma_{-8}$)	2.59	0.000	3.2*	
(**14**) 1.2,3.4,5.6,7.8-Tetrabenzanthracene[a] (D_{2h}, b_{3g})									
b_{2g} ($\pi_0^* \leftarrow \pi_{-1}$)	0.01	*l*	0.00		b_{3g} ($\pi_0^* \leftarrow \pi_{-6}$)	1.71	*l*	2.29	
a_u ($\pi_0^* \leftarrow \pi_{-2}$)	0.32	0.003	0.70		b_{1u} ($\pi_0^* \leftarrow \pi_{-7}$)	1.77	0.038	2.29	
b_{2g} ($\pi_0^* \leftarrow \pi_{-3}$)	0.70	*l*	0.99		b_{2g} ($\pi_0^* \leftarrow \pi_{-8}$)	2.06	*l*	2.44	
b_{1u} ($\pi_0^* \leftarrow \pi_{-4}$)	1.37	0.360	1.29		a_g ($\pi_0^* \leftarrow \sigma_{-10}$)	2.45	*l*	3.3*	
a_u ($\pi_0^* \leftarrow \pi_{-5}$)	1.50	0.080	1.75						
(**15**) 3.4-Benzotetraphene (C_s, a″)									
a″ ($\pi_0^* \leftarrow \pi_{-1}$)	0.75	0.007	0.74		a″ ($\pi_1^* \leftarrow \pi_0$)	(2.34)	0.016		
a″ ($\pi_0^* \leftarrow \pi_{-2}$)	1.06	0.111	1.04		a″ ($\pi_0^* \leftarrow \pi_{-5}$)	2.47	0.011	2.76	
a″ ($\pi_0^* \leftarrow \pi_{-3}$)	1.65	0.025	1.87		a′ ($\pi_0^* \leftarrow \sigma_{-7}$)	2.82	0.000	3.3*	
a″ ($\pi_0^* \leftarrow \pi_{-4}$)	1.87	0.007	2.15						
(**16**) Pentaphene (C_{2v}, b_2)									
a_2 ($\pi_0^* \leftarrow \pi_{-1}$)	0.17	0.003	0.13		a_2 ($\pi_2^* \leftarrow \pi_{-1}$)	(2.69)	0.001		2.55[k]
b_2 ($\pi_0^* \leftarrow \pi_{-3}$)	1.29	0.001	1.26	1.26[k]	b_2 ($\pi_1^* \leftarrow \pi_{-1}$)	(2.74)	0.103		2.92[k]
a_2 ($\pi_0^* \leftarrow \pi_{-2}$)	1.34	0.092	1.59	1.44[k]	b_2 ($\pi_0^* \leftarrow \pi_{-6}$)	2.80	0.005	3.01	
a_2 ($\pi_0^* \leftarrow \pi_{-5}$)	2.06	0.009	2.23	2.20[k]	b_1 ($\pi_0^* \leftarrow \sigma_{-7}$)	2.83	*l*	3.2*	
b_2 ($\pi_0^* \leftarrow \pi_{-4}$)	2.06	0.027	2.55	2.37[k]					
(**17**) 3.4-Benzopentaphene (C_s, a″)									
a″ ($\pi_0^* \leftarrow \pi_{-1}$)	0.28	0.003	0.26		a″ ($\pi_0^* \leftarrow \pi_{-6}$)	2.28	0.018	2.33	2.32
a″ ($\pi_0^* \leftarrow \pi_{-2}$)	0.89	0.130	0.94		a″ ($\pi_0^* \leftarrow \pi_{-7}$)	2.69	0.004	2.71	2.73
a″ ($\pi_0^* \leftarrow \pi_{-3}$)	1.26	0.008	1.53	1.69	a′ ($\pi_0^* \leftarrow \sigma_{-8}$)	2.77	0.000	3.2*	
a″ ($\pi_0^* \leftarrow \pi_{-4}$)	1.60	0.009	1.82	1.85	a″ ($\pi_0^* \leftarrow \pi_{-9}$)	2.97	0.045	3.04	
a″ ($\pi_0^* \leftarrow \pi_{-5}$)	1.96	0.013	2.33	2.15					
(**18**) 6.7-Benzopentaphene[a] (C_{2v}, b_2)									
a_2 ($\pi_0^* \leftarrow \pi_{-1}$)	0.22	0.012	0.18		b_2 ($\pi_0^* \leftarrow \pi_{-5}$)	1.96	0.106	2.07	
a_2 ($\pi_0^* \leftarrow \pi_{-2}$)	0.83	0.084	0.66		a_2 ($\pi_0^* \leftarrow \pi_{-6}$)	2.03	0.011	2.39	
b_2 ($\pi_0^* \leftarrow \pi_{-3}$)	1.26	0.013	1.42		b_2 ($\pi_0^* \leftarrow \pi_{-7}$)	2.40	0.009	2.66	
a_2 ($\pi_0^* \leftarrow \pi_{-4}$)	1.66	0.129	1.84		b_1 ($\pi_0^* \leftarrow \sigma_{-8}$)	2.69	*l*	3.0*	
(**19**) Anthraceno-(2′.1′:1.2)-anthracene (C_{2h}, a_u)									
b_g ($\pi_0^* \leftarrow \pi_{-1}$)	0.91	0.177	0.72		b_g ($\pi_0^* \leftarrow \pi_{-5}$)	2.28	0.024	2.57	
a_u ($\pi_0^* \leftarrow \pi_{-2}$)	1.00	*l*	0.86		a_u ($\pi_0^* \leftarrow \pi_{-6}$)	2.56	*l*		
b_g ($\pi_0^* \leftarrow \pi_{-4}$)	1.69	0.018	1.82		a_u ($\pi_0^* \leftarrow \pi_{-7}$)	2.80	*l*		
a_u ($\pi_0^* \leftarrow \pi_{-3}$)	1.71	*l*	2.01		b_g ($\pi_3^* \leftarrow \pi_0$)	(3.02)	0.018		
b_g ($\pi_1^* \leftarrow \pi_0$)	(2.05)	0.013			a_g ($\pi_0^* \leftarrow \sigma_{-8}$)	3.03	0.000		
(**20**) 1.2,3.4-Dibenzotetracene[a](C_{2v}, a_2)									
a_2 ($\pi_0^* \leftarrow \pi_{-1}$)	0.75	0.029	0.84		b_1 ($\pi_0^* \leftarrow \pi_{-5}$)	2.19	0.055	2.51	
b_1 ($\pi_0^* \leftarrow \pi_{-2}$)	0.80	0.008	1.14		a_2 ($\pi_0^* \leftarrow \pi_{-6}$)	2.27	0.007	2.81	
a_2 ($\pi_0^* \leftarrow \pi_{-3}$)	1.59	0.231	1.69		a_2 ($\pi_1^* \leftarrow \pi_{-2}$)	(2.87)	0.261		
b_1 ($\pi_0^* \leftarrow \pi_{-4}$)	1.82	0.000	2.11		b_2 ($\pi_0^* \leftarrow \sigma_{-8}$)	2.89	0.000	3.4*	
b_1 ($\pi_1^* \leftarrow \pi_0$)	(2.05)	0.000							
(**21**) 1.2,7.8-Dibenzotetracene (C_{2h}, a_u)									
a_u ($\pi_0^* \leftarrow \pi_{-1}$)	0.62	*l*	0.74		a_u ($\pi_0^* \leftarrow \pi_{-5}$)	2.23	*l*	2.60	
b_g ($\pi_0^* \leftarrow \pi_{-2}$)	0.97	0.049	1.19		b_g ($\pi_1^* \leftarrow \pi_{-1}$)	(2.76)	0.185		
b_g ($\pi_0^* \leftarrow \pi_{-3}$)	1.37	0.136	1.64		a_u ($\pi_1^* \leftarrow \pi_{-2}$)	(2.85)	*l*		
a_u ($\pi_0^* \leftarrow \pi_{-4}$)	1.69	*l*	1.96		a_g ($\pi_0^* \leftarrow \sigma_{-8}$)	3.00	0.000	3.4*	
b_g ($\pi_1^* \leftarrow \pi_0$)	(2.07)	0.026							
(**22**) Heptaphene[a] (C_{2v},b_2)									
a_2 ($\pi_0^* \leftarrow \pi_{-1}$)	0.44	0.107	0.00		b_2 ($\pi_2^* \leftarrow \pi_{-1}$)	(2.38)	0.008		
b_2 ($\pi_0^* \leftarrow \pi_{-2}$)	1.27	0.015	1.23		b_2 ($\pi_0^* \leftarrow \pi_{-6}$)	2.49	0.031	2.65	
a_2 ($\pi_0^* \leftarrow \pi_{-3}$)	1.44	0.225	1.23		a_2 ($\pi_2^* \leftarrow \pi_0$)	(2.51)	0.421		
a_2 ($\pi_0^* \leftarrow \pi_{-4}$)	1.76	0.046	1.96		a_2 ($\pi_0^* \leftarrow \pi_{-7}$)	2.69	0.015	2.86	
b_2 ($\pi_0^* \leftarrow \pi_{-5}$)	1.91	0.032	1.96		a_2 ($\pi_0^* \leftarrow \pi_{-8}$)	2.95	0.007	3.0	
b_2 ($\pi_2^* \leftarrow \pi_{-1}$)	(1.99)	0.001			b_2 ($\pi_0^* \leftarrow \pi_{-9}$)	3.11	0.006	3.2	
a_2 ($\pi_1^* \leftarrow \pi_{-1}$)	(2.21)	0.347							
(**23**) 1.2-Benzopentacene (C_s, a″)									
a″ ($\pi_0^* \leftarrow \pi_{-1}$)	0.96	0.021	1.12		a″ ($\pi_0^* \leftarrow \pi_{-5}$)	2.50	0.023	2.81	
a″ ($\pi_0^* \leftarrow \pi_{-2}$)	1.31	0.146	1.23		a″ ($\pi_1^* \leftarrow \pi_{-2}$)	(2.54)	0.141		
a″ ($\pi_1^* \leftarrow \pi_0$)	(1.43)	0.033			a″ ($\pi_2^* \leftarrow \pi_0$)	(2.80)	0.002		
a″ ($\pi_0^* \leftarrow \pi_{-3}$)	1.80	0.006	2.02		a″ ($\pi_0^* \leftarrow \pi_{-6}$)	2.87	0.002	3.14	
a″ ($\pi_0^* \leftarrow \pi_{-4}$)	2.05	0.007	2.34		a″ ($\pi_0^* \leftarrow \pi_{-7}$)	3.23	0.000	3.47	
a″ ($\pi_1^* \leftarrow \pi_{-1}$)	(2.30)	0.052			a′ ($\pi_0^* \leftarrow \sigma_{-8}$)	3.25	0.000	3.59	

TABLE 1: Continued

state (transition)	calculation: excitation energy[b]	calculation: oscillator strength	experiment: PE[c]	experiment: electronic absorption[d]	state (transition)	calculation: excitation energy[b]	calculation: oscillator strength	experiment: PE[c]	experiment: electronic absorption[d]
(**24**) 8.9-Benzopicene (C_s, a″)									
a″ (π_0* ← π_{-1})	0.19	0.002	0.42		a″ (π_0* ← π_{-5})	1.88	0.019	2.24	
a″ (π_0* ← π_{-2})	0.94	0.083	0.94		a″ (π_0* ← π_{-6})	2.50	0.004	2.79	
a″ (π_0* ← π_{-3})	1.13	0.073	1.40		a″ (π_0* ← π_{-7})	2.53	0.039	2.79	
a″ (π_0* ← π_{-4})	1.61	0.004	1.86		a′ (π_0* ← σ_{-8})	2.57	0.000	3.07	
(**25**) Triphenylene[a] (C_s, a″)									
a″ (π_0* ← π_{-1})	0.03	0.000	0.00		a″ (π_0* ← π_{-4})	1.81	0.060	1.79	1.94
a″ (π_0* ← π_{-2})	0.72	0.022	0.77	0.72	a″ (π_0* ← π_{-5})	2.16	0.116	2.17	2.13
a″ (π_0* ← π_{-3})	1.59	0.001	1.79	1.75	a′ (π_0* ← σ_{-6})	2.36	0.000	2.8*	

[a] Tamm−Dancoff approximation is used in the TDDFT calculation. [b] The parenthesis designates a satellite transition as described at the beginning of section 3. [c] Photoelectron spectra; taken from Boschi, Clar, and Schmidt.[53] The asterisk represents an onset of σ ionization manifold. [d] Taken from Shida,[30] unless otherwise noted. [e] Taken from Szczepanski et al.[37] [f] Taken from Szczepanski et al.[42] [g] Taken from Salama, Joblin, and Allamandola.[43] [h] Taken from Szczepanski, Wehlburg, and Vala.[41] [i] Taken from Halasinski et al.[45] [j] Taken from Salama, Joblin, and Allamandola.[38] [k] Taken from Khan.[26,28] [l] Forbidden.

large. It may be that the calculated lowest $\pi^* \leftarrow \sigma$ transition is associated with a σ orbital that is only weakly bonding and is therefore not primarily responsible for the σ manifold onset or that it is isolated from a dense population of higher-lying $\pi^* \leftarrow \sigma$ transitions.

Sterically overcrowded hydrocarbons such as 3.4,5.6-dibenzophenanthrene (**8**) and biphenyl (**48**) undergo a significant out-of-plane structural distortion, causing the σ and π orbitals (so designated for a planar structure) to become indistinct from one another. Nonetheless, TDDFT is capable of describing the excited states of these nonplanar PAH radical cations with comparable accuracy to the planar species. This again attests to the balanced treatment of σ and π orbitals (and mixtures thereof) by TDDFT. A previous CASPT2 calculation[57] of the biphenyl radical cation (**48**) predicted the vertical excitation energies of the four lowest excited states to be 1.08, 1.26, 1.88, and 3.21 eV, respectively, at the (nearly) planar cation geometry. Rubio et al.[57] assigned the third and fourth lowest excitations to the measured electronic absorption bands at 1.76 and 3.20 eV and interpreted the relatively large deviations between the calculated excitation energies to the two lowest states and the photoelectron data (0.70 and 0.86 eV) as a consequence of the twisted geometry of the neutral species. The present TDDFT calculation supports both conclusions. The two lowest-lying transitions computed by TDDFT at the twisted neutral geometry are significantly lower than those predicted by CASPT2 at the planar cation geometry. The oscillator strengths for these transitions predicted by TDDFT are small, and these transitions are likely invisible in the electronic absorption spectra.

Occasionally, negative excitation energies from the Tamm−Dancoff TDDFT calculations were found. In all cases, they are caused by the Kohn−Sham self-consistent field (SCF) procedure for the reference state converging to a higher energy with a different symmetry symbol than that of the true ground state. Therefore, for consistency, a different initial orbital guess was chosen and Kohn−Sham SCF calculation was rerun to ensure that the true ground-state solution is obtained prior to subsequent TDDFT calculations. However, redesignating the lowest excited state, with the negative excitation energy, as the ground state permits the measured photoelectron peaks to be correlated with the calculated results in a straightforward fashion. The agreement between the calculated and experimental data is accurate (not shown), which indicates that the interpretation is valid. The accurate agreement is because these excited-state reference wave functions are of predominantly single-determinant character and are represented by DFT as accurately as the ground-state solutions. It is fascinating to observe the robustness of linear response theory to various physical situations; negative excitation energies obtained from (Tamm−Dancoff) TDDFT for an excited-state reference can be viewed as a stimulated emission of radiation. This further suggests that an application of (Tamm−Dancoff) TDDFT from a one- or two-electron excited state will allow access to two-electron excited states (multiphoton excitations) that are outside the determinant space spanned by adiabatic TDDFT based on the aufbau reference wave function.

As evident in Table 3, the accuracy of the TDDFT excitation energies is hardly affected by the presence of nonbenzenoid or noncondensed aromatic rings. The agreement between the calculated excitation energies and the measured photoelectron or electronic absorption band positions is excellent for both the $\pi^* \leftarrow \pi$ and $\pi^* \leftarrow \sigma$ transitions. The ordering of Koopmans and satellite peaks [e.g., acepleiadylene (**45**) and pleiadiene (**46**)] and the oscillator strengths are also consistent with the experimental findings. Table 4 shows that TDDFT maintains the accuracy of the vertical excitation energies for heteronuclear PAH radical cations and that the calculated oscillator strengths are consistent with the experimental data. However, the subtle differences in the excitation energies among the three related compounds (dibenzofuran, carbazole, and dibenzothiophene) are not reproduced. The sulfur atom in dibenzothiophene (**51**) is known to act like the CH═CH group electronically,[55] and consequently, the patterns of experimental excitation energies are very similar for dibenzothiophene and phenanthrene (**5**) and consistent with the results of TDDFT calculations. Compared to that of phenanthrene, however, the calculated σ ionization onsets of dibenzothiophene and dibenzofuran exhibit larger deviations from experiment. Charge transfer effects, which are not well described by TDDFT, may become relatively more important by the presence of heteronuclei and may be the cause of the larger deviations.

Vertical excitation energies of the radical anions of tetracene (**2**), pentacene (**3**), chrysene (**6**), perylene (**26**), pyrene (**30**), azulene (**41**), and biphenylene (**47**) were also computed. Despite the nonphysical exponential falloff of the BLYP potentials in the asymptotic regions,[73,74] the calculated excitation energies of the several lowest bands match closely with the experimental data. This is probably due to the valence character of these excited states, which are comparatively compact spatially and are not affected significantly by the shape of the exchange−correlation potentials in the asymptotic region. The main spectral features of the radical anion of an alternant hydrocarbon are

TABLE 2: Vertical Excitation Energies (eV) and Oscillator Strengths of Peri-Condensed Aromatic Hydrocarbon Radical Cations

	calculation		experiment			calculation		experiment	
state (transition)	excitation energy[b]	oscillator strength	PE[c]	electronic absorption[d]	state (transition)	excitation energy[b]	oscillator strength	PE[c]	electronic absorption[d]
				(**26**) Perylene (D_{2h}, a_u)					
b_{2g} ($\pi_0^* \leftarrow \pi_{-1}$)	1.45	0.000	1.55	1.54, 1.56,[e] 1.57[f]	b_{2g} ($\pi_0^* \leftarrow \pi_{-4}$)	1.86	0.028	1.90	1.92, 1.93,[e] 1.91[g]
b_{1u} ($\pi_0^* \leftarrow \pi_{-2}$)	1.60	*l*	1.68		b_{3g} ($\pi_0^* \leftarrow \pi_{-3}$)	2.48	0.321	2.34	2.28, 2.32,[e] 2.36,[f] 2.29[g]
b_{3g} ($\pi_1^* \leftarrow \pi_0$)	(1.74)	0.014		1.69, 1.69,[e] 1.71,[f] 1.69[g]	a_g ($\pi_0^* \leftarrow \sigma_{-5}$)	3.13	*l*	3.4*	
				(**27**) 1.12-Benzoperylene (C_{2v}, a_2)					
b_2 ($\pi_0^* \leftarrow \pi_{-1}$)	0.60	0.001	0.67		b_2 ($\pi_0^* \leftarrow \pi_{-5}$)	2.38	0.000	2.69	
a_2 ($\pi_0^* \leftarrow \pi_{-2}$)	1.39	0.001	1.51	1.51, 1.31,[g] 1.51[h]	b_2 ($\pi_1^* \leftarrow \pi_0$)	(2.67)	0.142		2.41, 2.40,[g] 2.47[h]
b_2 ($\pi_0^* \leftarrow \pi_{-3}$)	1.71	0.056	1.66	1.61, 1.62,[g] 1.63[h]	a_1 ($\pi_0^* \leftarrow \sigma_{-6}$)	2.84	*l*		
a_2 ($\pi_0^* \leftarrow \pi_{-4}$)	1.73	0.027	1.86	1.84, 1.84[g]					
				(**28**) Coronene (D_{2h}, a_u)					
b_{1u} ($\pi_0^* \leftarrow \pi_{-1}$)	0.01	*l*	0.00		b_{3g} ($\pi_0^* \leftarrow \pi_{-4}$)	1.65	0.055	1.83	1.62[g]
b_{3g} ($\pi_0^* \leftarrow \pi_{-2}$)	1.14	0.002	1.29	1.29, 1.31,[g] 1.32,[h] 1.29[i]	b_{2g} ($\pi_0^* \leftarrow \pi_{-5}$)	1.69	0.023	1.83	1.77, 1.77[g]
b_{2g} ($\pi_0^* \leftarrow \pi_{-3}$)	1.21	0.006	1.29	1.46, 1.47[g]	b_{1g} ($\pi_0^* \leftarrow \sigma_{-6}$)	2.55	0.000	3.0*	
				(**29**) Ovalene (D_{2h}, b_{2g})					
b_{3g} ($\pi_0^* \leftarrow \pi_{-1}$)	0.58	*l*	0.60		b_{2g} ($\pi_0^* \leftarrow \pi_{-6}$)	2.02	*l*	2.14	
a_u ($\pi_0^* \leftarrow \pi_{-2}$)	1.16	0.029	1.22	1.10[j]	b_{1u} ($\pi_1^* \leftarrow \pi_0$)	(2.22)	0.112		2.21[j]
b_{1u} ($\pi_0^* \leftarrow \pi_{-3}$)	1.43	0.020	1.44	1.27[j]	b_{3g} ($\pi_0^* \leftarrow \pi_{-7}$)	2.54	*l*	2.89	
b_{1u} ($\pi_0^* \leftarrow \pi_{-4}$)	1.64	0.007	1.88		a_u ($\pi_2^* \leftarrow \pi_0$)	(2.63)	0.013		2.68[j]
a_u ($\pi_0^* \leftarrow \pi_{-5}$)	1.86	0.016	1.88		a_g ($\pi_0^* \leftarrow \sigma_{-8}$)	2.87	*l*		
				(**30**) Pyrene (D_{2h}, b_{2g})					
b_{3g} ($\pi_0^* \leftarrow \pi_{-1}$)	0.85	*l*	0.85		b_{1u} ($\pi_0^* \leftarrow \pi_{-4}$)	2.38	0.018	2.55	2.51, 2.53,[g] 2.55[k]
b_{1u} ($\pi_0^* \leftarrow \pi_{-2}$)	1.55	0.015	1.59	1.56, 1.55,[g] 1.58[k]	b_{1g} ($\pi_0^* \leftarrow \sigma_{-5}$)	2.78	*l*	3.1*	
a_u ($\pi_0^* \leftarrow \pi_{-3}$)	2.01	0.018	1.88	1.87, 1.88,[g] 1.74[k]					
				(**31**) 1.2-Benzopyrene[a] (C_{2v}, b_1)					
a_2 ($\pi_0^* \leftarrow \pi_{-1}$)	0.47	0.002	0.61		a_2 ($\pi_0^* \leftarrow \pi_{-4}$)	2.25	0.022	2.33	
a_2 ($\pi_0^* \leftarrow \pi_{-2}$)	1.15	0.006	1.33	1.34[g]	b_1 ($\pi_0^* \leftarrow \pi_{-5}$)	2.27	0.031	2.42	2.58[g]
b_1 ($\pi_0^* \leftarrow \pi_{-3}$)	1.49	0.076	1.48		b_2 ($\pi_0^* \leftarrow \sigma_{-6}$)	2.69	*l*	3.1*	
				(**32**) 3.4-Benzopyrene (C_s, a″)					
a″ ($\pi_0^* \leftarrow \pi_{-1}$)	0.89	0.004	0.88	0.95	a″ ($\pi_1^* \leftarrow \pi_0$)	(2.38)	0.067		2.23, 2.24[g]
a″ ($\pi_0^* \leftarrow \pi_{-2}$)	1.60	0.047	1.61	1.58, 1.59[g]	a″ ($\pi_0^* \leftarrow \pi_{-5}$)	2.74	0.105	2.83	2.76, 2.77[g]
a″ ($\pi_0^* \leftarrow \pi_{-3}$)	1.70	0.013	1.80	1.73	a′ ($\pi_0^* \leftarrow \sigma_{-6}$)	2.90	0.000	3.3*	
a″ ($\pi_0^* \leftarrow \pi_{-4}$)	2.11	0.015	2.37	1.91, 1.91[g]					
				(**33**) 1.2,6.7-Dibenzopyrene (D_{2h}, b_{3g})					
b_{2g} ($\pi_0^* \leftarrow \pi_{-1}$)	0.30	*l*	0.43		b_{1u} ($\pi_0^* \leftarrow \pi_{-5}$)	2.17	0.026	2.44	
a_u ($\pi_0^* \leftarrow \pi_{-2}$)	0.57	0.005	0.84		b_{3g} ($\pi_0^* \leftarrow \pi_{-6}$)	2.28	*l*	2.44	
b_{1u} ($\pi_0^* \leftarrow \pi_{-3}$)	1.24	0.083	1.27		a_u ($\pi_0^* \leftarrow \pi_{-7}$)	2.28	0.018		
b_{2g} ($\pi_0^* \leftarrow \pi_{-4}$)	1.32	*l*	1.79		a_g ($\pi_0^* \leftarrow \sigma_{-8}$)	2.52	*l*	2.5*	
				(**34**) 3.4,9.10-Dibenzopyrene (C_{2v}, b_2)					
a_2 ($\pi_0^* \leftarrow \pi_{-1}$)	0.63	0.009	0.74		a_2 ($\pi_1^* \leftarrow \pi_0$)	(2.37)	0.211		2.20[g]
b_2 ($\pi_0^* \leftarrow \pi_{-3}$)	1.48	0.000	1.52	1.53[g]	a_2 ($\pi_0^* \leftarrow \pi_{-6}$)	2.55	0.079	2.84	2.87[g]
a_2 ($\pi_0^* \leftarrow \pi_{-2}$)	1.52	0.066	1.97	2.04[g]	b_2 ($\pi_1^* \leftarrow \pi_{-1}$)	(2.80)	0.004		
b_2 ($\pi_0^* \leftarrow \pi_{-4}$)	1.76	0.005	1.97		b_1 ($\pi_0^* \leftarrow \sigma_{-7}$)	2.88	*l*		
b_2 ($\pi_0^* \leftarrow \pi_{-5}$)	2.26	0.025	2.51	2.41[g]					
				(**35**) Dinaphtho-(2′.3′:1.2);(2″.3″:6.7)-pyrene (D_{2h}, b_{2g})					
a_u ($\pi_0^* \leftarrow \pi_{-1}$)	0.16	0.008	0.21		b_{3g} ($\pi_0^* \leftarrow \pi_{-6}$)	1.84	*l*	2.05	
b_{3g} ($\pi_0^* \leftarrow \pi_{-2}$)	0.23	*l*	0.21		b_{2g} ($\pi_0^* \leftarrow \pi_{-7}$)	2.15	*l*	2.38	
b_{1u} ($\pi_0^* \leftarrow \pi_{-4}$)	1.09	0.000	1.14		b_{1u} ($\pi_0^* \leftarrow \pi_{-8}$)	2.23	0.019	2.38	
b_{2g} ($\pi_0^* \leftarrow \pi_{-3}$)	1.17	*l*	1.14		a_u ($\pi_0^* \leftarrow \pi_{-9}$)	2.56	0.003		
a_u ($\pi_0^* \leftarrow \pi_{-5}$)	1.65	0.131	1.77		a_g ($\pi_0^* \leftarrow \sigma_{-10}$)	2.62	*l*		
				(**36**) 1.14,4.5-Dibenzopentacene (C_{2v}, a_2)					
b_1 ($\pi_0^* \leftarrow \pi_{-1}$)	0.05	0.000	0.41		b_1 ($\pi_0^* \leftarrow \pi_{-5}$)	2.12	0.021	2.43	
a_2 ($\pi_0^* \leftarrow \pi_{-2}$)	0.91	0.049	1.10		a_2 ($\pi_0^* \leftarrow \pi_{-6}$)	2.27	0.011	2.43	
b_1 ($\pi_0^* \leftarrow \pi_{-3}$)	1.36	0.001	1.47		b_1 ($\pi_0^* \leftarrow \pi_{-7}$)	2.40	0.002	3.00	
a_2 ($\pi_0^* \leftarrow \pi_{-4}$)	1.53	0.068	1.70		b_1 ($\pi_1^* \leftarrow \pi_{-2}$)	(2.72)	0.002		
a_2 ($\pi_1^* \leftarrow \pi_{-1}$)	(1.92)	0.000			b_2 ($\pi_0^* \leftarrow \sigma_{-8}$)	2.73	0.000	3.3*	
a_2 ($\pi_1^* \leftarrow \pi_{-1}$)	(2.05)	0.142							
				(**37**) Anthanthrene (C_{2h}, a_u)					
a_u ($\pi_0^* \leftarrow \pi_{-2}$)	1.19	*l*	1.16		a_u ($\pi_0^* \leftarrow \pi_{-4}$)	2.33	*l*	2.50	
b_g ($\pi_0^* \leftarrow \pi_{-1}$)	1.31	0.032	1.30		b_g ($\pi_1^* \leftarrow \pi_0$)	(2.50)	0.196		
b_g ($\pi_0^* \leftarrow \pi_{-3}$)	1.78	0.001	1.8		a_u ($\pi_1^* \leftarrow \pi_{-2}$)	(3.02)	*l*		
b_g ($\pi_0^* \leftarrow \pi_{-5}$)	2.31	0.030	2.50		a_g ($\pi_0^* \leftarrow \sigma_{-6}$)	3.03	0.000	3.42*	
				(**38**) Pyreno-(1.3:10′.2′)-pyrene (C_{2h}, b_g)					
b_g ($\pi_0^* \leftarrow \pi_{-1}$)	0.69	*l*	0.77		a_u ($\pi_1^* \leftarrow \pi_0$)	(2.49)	0.236		
a_u ($\pi_0^* \leftarrow \pi_{-2}$)	1.07	0.031	1.20		a_u ($\pi_0^* \leftarrow \pi_{-7}$)	2.60	0.040	2.92	
a_u ($\pi_0^* \leftarrow \pi_{-3}$)	1.52	0.045	1.66		b_g ($\pi_0^* \leftarrow \pi_{-6}$)	2.62	*l*	2.92	
a_u ($\pi_0^* \leftarrow \pi_{-4}$)	1.62	0.037	1.66		b_g ($\pi_0^* \leftarrow \pi_{-8}$)	2.80	*l*	3.40	
b_g ($\pi_0^* \leftarrow \pi_{-5}$)	1.89	*l*	2.22		a_g ($\pi_0^* \leftarrow \sigma_{-9}$)	2.82	*l*	3.7*	

TABLE 2: Continued

state (transition)	calculation: excitation energy[b]	calculation: oscillator strength	experiment: PE[c]	experiment: electronic absorption[d]	state (transition)	calculation: excitation energy[b]	calculation: oscillator strength	experiment: PE[c]	experiment: electronic absorption[d]
(**39**) Peropyrene (D_{2h}, b_{2g})									
b_{3g} ($\pi_0^* \leftarrow \pi_{-1}$)	1.07	*l*	1.04		a_u ($\pi_1^* \leftarrow \pi_0$)	(2.28)	0.459		
a_u ($\pi_0^* \leftarrow \pi_{-2}$)	1.41	0.037	1.43		b_{2g} ($\pi_0^* \leftarrow \pi_{-6}$)	2.45	*l*	2.47	
b_{3g} ($\pi_0^* \leftarrow \pi_{-3}$)	1.80	*l*	2.01		b_{1u} ($\pi_2^* \leftarrow \pi_0$)	(2.90)	0.000		
b_{1u} ($\pi_0^* \leftarrow \pi_{-4}$)	1.83	0.003	2.01		b_{1g} ($\pi_0^* \leftarrow \sigma_{-7}$)	2.96	*l*	3.37*	
b_{1u} ($\pi_0^* \leftarrow \pi_{-5}$)	2.13	0.024	2.33						
(**40**) Dinaphtho-(2′.8′:2.4);(1″.7″:10.8)-coronene (C_{2h}, a_u)									
a_u ($\pi_0^* \leftarrow \pi_{-1}$)	0.73	*l*	0.69		a_u ($\pi_0^* \leftarrow \pi_{-8}$)	2.46	*l*	2.61	
b_g ($\pi_0^* \leftarrow \pi_{-2}$)	1.00	0.087	1.02		b_g ($\pi_0^* \leftarrow \pi_{-7}$)	2.47	0.037	2.94	
b_g ($\pi_0^* \leftarrow \pi_{-3}$)	1.55	0.002	1.70		b_g ($\pi_2^* \leftarrow \pi_0$)	(2.53)	0.007		
b_g ($\pi_0^* \leftarrow \pi_{-4}$)	1.65	0.009	1.83		a_u ($\pi_3^* \leftarrow \pi_0$)	(2.58)	*l*		
a_u ($\pi_0^* \leftarrow \pi_{-5}$)	1.74	*l*	2.00		a_u ($\pi_0^* \leftarrow \pi_{-9}$)	2.73	*l*		
b_g ($\pi_0^* \leftarrow \pi_{-6}$)	1.81	0.009	2.14		a_u ($\pi_3^* \leftarrow \pi_0$)	(2.87)	*l*		
b_g ($\pi_1^* \leftarrow \pi_0$)	(2.06)	0.098			a_g ($\pi_0^* \leftarrow \sigma_{-10}$)	2.93	0.000	3.6*	

[a] Tamm−Dancoff approximation is used in the TDDFT calculation. [b] The parenthesis designates a satellite transition as described at the beginning of section 3. [c] Photoelectron spectra; taken from Boschi, Clar, and Schmidt.[53] The asterisk represents an onset of σ ionization manifold. [d] Taken from Shida,[30] unless otherwise noted. [e] Taken from Szczepanski, Chapo, and Vala.[35] [f] Taken from Joblin, Salama, and Allamandola.[40] [g] Taken from Khan.[31] [h] Taken from Salama, Joblin, and Allamandola.[43] [i] Taken from Szczepanski and Vala.[17] [j] Taken from Ruiterkamp et al.[46] [k] Taken from Vala et al.[39] [l] Forbidden.

very similar to those of its corresponding radical cation (cf. ref 22), which is a consequence of the Coulson−Rushbrooke pairing theorem.[75] For alternant hydrocarbons, there is particle−hole equivalence in Hückel theory. Thus a radical cation and radical anion are predicted to have identical spectra. Closer inspection of the spectra reveals some shifts in the band positions on going from the cation to the anion, the cause of which is not immediately known. Shida and Iwata[22] conjectured that these shifts arise from the σ orbital interleaving in both ions. The present TDDFT calculations performed for the cation and anion at the neutral geometry appear to reproduce the sign and magnitude of these shifts, at least for the most intense band of each species. For instance, the 1.43-eV band of the tetracene cation undergoes a blue shift of 0.07 eV, and the TDDFT calculation predicts a blue shift of 0.05 eV. Similarly, the 1.30-eV band of the pentacene cation is blue-shifted by 0.11 eV, as compared to the 0.08 eV shift from TDDFT. Hence these results support the Shida−Iwata hypothesis. For these radical anions, transitions to σ^* orbitals appear to play more important roles relative to those of the radical cations, and the calculated $\sigma^* \leftarrow \pi$ transitions are consistent with the experimental data in terms of positions and intensities.

Comparing the calculated and measured spectra of structurally similar PAH radical cations, we notice that TDDFT appears to reproduce relative and subtle spectral differences between them more accurately than one would expect from its typical absolute accuracy. For instance, 3.4-benzopentaphene (**17**) and 6.7-benzopentaphene (**18**) differ structurally from each other just in the position of an extra benzene ring attached to their pentaphene backbone, and accordingly, the distributions of low-lying excited states of both radical cations look similar with minor differences. The lowest four $\pi^* \leftarrow \pi$ transitions occur at 0.26, 0.94, 1.53, and 1.82 eV in the 3.4-benzopentaphene radical cation and 0.18, 0.66, 1.42, and 1.84 eV in the 6.7-benzopentaphene radical cations. TDDFT tends to underestimate the differences in the transition energies between the corresponding states of the two radical cations, but the signs of the differences are correctly reproduced. Likewise, TDDFT predicts the signs of spectral differences in the four lowest transitions between the radical cations of 1.2,3.4-dibenzotetracene (**20**) and 1.2,7.8-dibenzotetracene (**21**).

Anthracene (**1**), tetracene (**2**), pentacene (**3**), and hexacene (**4**) have linearly connected benzene rings, and their spectroscopic properties are often discussed collectively. The photoelectron peaks of these species are straightforwardly assigned to the calculated Koopmans transition energies. The positions of the prominent electronic absorption bands of their radical cations are also in good agreement with the calculated excitation energies and intensity patterns for the anthracene, tetracene, and pentacene radical cations. Some of these intense electronic absorption bands are assigned to satellite transitions, and the degree of agreement does not seem to be affected by the nature of the transitions. The pentacene radical cation was studied previously by Halasinski et al. using TDDFT.[45] They reassigned an electronic absorption band at 2.92 eV to a satellite ^2a_u state on the basis of an intensity argument. This band was originally assigned to a Koopmans $^2b_{1u}$ state by Szczepanski et al.[41] The present TDDFT result parallels that of Halasinski et al., predicting the satellite transition to the ^2a_u state to have a greater intensity than that to the Koopmans $^2b_{1u}$ state. However, because the method of calculation used in this study is very similar to what was used by Halasinski et al., the present study does not resolve this question. It has been experimentally deduced that the lowest excited state of the pentacene and hexacene radical cations is predominantly a satellite state,[76] whereas that of the anthracene radical cation is a Koopmans state. The present calculation strongly supports these conclusions, which are, however, contradicted by a previous many-body Green's function study.[59] The situation for the tetracene radical cation has been ambiguous, but according to TDDFT, the lowest excited state of this species is a Koopmans state. Although the electronic absorption spectrum of the hexacene radical cation is not available, we can safely expect (by virtue of the Coulson−Rushbrooke pairing theorem) that the electronic absorption spectrum of the hexacene radical anion[76] will correlate with the calculated excitation energies of the radical cation. Indeed, three of the most intense bands (labeled 2, 5, and 6 in the original figure[76]) experimentally observed at 1.2, 2.8, and 3.2 eV correspond accurately to the calculated excitation energies of 1.24, 2.87, and 3.11 (or 3.35) eV that have large intensities.

Previously, we studied the excitation energies of the radical cations of naphthalene, anthracene (**1**), pyrene (**30**), and perylene (**26**) calculated at the optimized geometries of the respective radical cations.[67] Despite the overall excellent agreement between experiment and theory, the calculated excitation energies to the lowest-lying excited state of each species tended

TABLE 3: Vertical Excitation Energies (eV) and Oscillator Strengths of Nonbenzenoid or Noncondensed Aromatic Hydrocarbon Radical Cations

state (transition)	calculation: excitation energy[a]	calculation: oscillator strength	experiment: PE[b]	experiment: electronic absorption[c]
(**41**) Azulene (C_{2v}, a_2)				
b_1 ($\pi_0^* \leftarrow \pi_{-1}$)	1.04	0.000	1.07	
a_2 ($\pi_0^* \leftarrow \pi_{-2}$)	2.58	0.002	2.64	2.58
b_1 ($\pi_1^* \leftarrow \pi_0$)	(2.76)	0.001		
b_1 ($\pi_0^* \leftarrow \pi_{-3}$)	3.24	0.009	3.42	3.37
a_1 ($\pi_0^* \leftarrow \sigma_{-4}$)	3.24	*e*	3.6*	
(**42**) Acenaphthylene (C_{2v}, b_2)				
a_2 ($\pi_0^* \leftarrow \pi_{-1}$)	0.33	0.002	0.17	0.59
b_2 ($\pi_0^* \leftarrow \pi_{-2}$)	0.63	0.001	0.77	0.80
b_1 ($\pi_0^* \leftarrow \sigma_{-3}$)	2.46	*e*	2.5*	
a_2 ($\pi_0^* \leftarrow \pi_{-4}$)	2.55	0.001	2.65	2.53
(**43**) Acenaphthene (C_{2v}, a_2)				
b_2 ($\pi_0^* \leftarrow \pi_{-1}$)	1.02	0.000	0.98	
b_2 ($\pi_0^* \leftarrow \pi_{-2}$)	2.06	0.039	1.94	1.88, 1.89[d]
a_2 ($\pi_0^* \leftarrow \pi_{-3}$)	2.70	0.030	2.7	2.74, 2.88[d]
a_1 ($\pi_0^* \leftarrow \sigma_{-4}$)	2.88	*e*	2.9*	
(**44**) Fluoranthene (C_{2v}, a_2)				
b_1 ($\pi_0^* \leftarrow \pi_{-1}$)	0.16	0.000	0.15	
b_1 ($\pi_0^* \leftarrow \pi_{-2}$)	0.90	0.000	0.92	
a_2 ($\pi_0^* \leftarrow \pi_{-3}$)	1.54	0.071	1.55	1.46
b_1 ($\pi_0^* \leftarrow \pi_{-4}$)	2.23	0.018	2.44	2.44
a_1 ($\pi_0^* \leftarrow \sigma_{-5}$)	2.61	*e*	2.9*	
(**45**) Acepleiadylene (C_{2v}, a_2)				
b_1 ($\pi_0^* \leftarrow \pi_{-1}$)	0.48	0.000	0.70	
b_1 ($\pi_0^* \leftarrow \pi_{-2}$)	1.47	0.002	1.64	
a_2 ($\pi_0^* \leftarrow \pi_{-3}$)	2.15	0.003	2.38	
b_1 ($\pi_2^* \leftarrow \pi_0$)	(2.49)	0.002		
a_2 ($\pi_1^* \leftarrow \pi_0$)	(2.54)	0.007		
b_1 ($\pi_0^* \leftarrow \pi_{-4}$)	2.76	0.003	2.74	
b_2 ($\pi_0^* \leftarrow \sigma_{-5}$)	3.03	0.000	3.4*	
(**46**) Pleiadiene (C_{2v}, a_2)				
b_1 ($\pi_0^* \leftarrow \pi_{-1}$)	1.79	0.000	1.76	
b_1 ($\pi_1^* \leftarrow \pi_0$)	(1.95)	0.003		
a_2 ($\pi_0^* \leftarrow \pi_{-2}$)	2.30	0.028	2.40	
b_1 ($\pi_0^* \leftarrow \pi_{-3}$)	2.50	0.027	2.40	
a_2 ($\pi_2^* \leftarrow \pi_0$)	(2.91)	0.138		
b_1 ($\pi_3^* \leftarrow \pi_0$)	(3.51)	0.025		
b_2 ($\pi_0^* \leftarrow \sigma_{-4}$)	3.59	0.000	4.00*	
(**47**) Biphenylene (D_{2h}, b_{3g})				
a_u ($\pi_0^* \leftarrow \pi_{-1}$)	1.16	0.001	1.29	1.35
b_{2g} ($\pi_0^* \leftarrow \pi_{-2}$)	1.80	*e*	2.07	
b_{1u} ($\pi_0^* \leftarrow \pi_{-3}$)	2.47	0.092	2.47	2.33
b_{2g} ($\pi_1^* \leftarrow \pi_0$)	(2.88)	*e*		
b_{2u} ($\pi_0^* \leftarrow \sigma_{-4}$)	2.97	0.000	3.1*	
(**48**) Biphenyl (D_2, b_3)				
a ($0^* \leftarrow -1$)	0.58	0.000	0.70	
b_2 ($0^* \leftarrow -2$)	0.59	0.000	0.86	
b_1 ($0^* \leftarrow -3$)	1.77	0.151	1.48	1.76
b_1 ($0^* \leftarrow -4$)	2.46	0.018	2.83	3.20

[a] The parenthesis designates a satellite transition as described at the beginning of section 3. [b] Photoelectron spectra; taken from Boschi, Clar, and Schmidt.[53] The asterisk represents an onset of σ ionization manifold. [c] Taken from Shida,[30] unless otherwise noted. [d] Taken from Banisaukas et al.[49] [e] Forbidden.

to be higher than those from the photoelectron data. The present TDDFT calculations performed at the neutral geometries yield excitation energies of the lowest excited states of these species systematically lower than those previously obtained at the cation geometries and are in appreciably better agreement with experiment. Because the photoelectron transitions occur at neutral geometries, this result suggests that TDDFT may be able to account for the slight spectral differences arising from the geometry changes (cf. the discussions on biphenyl radical cation). In the previous study on the perylene radical cation, an intense electronic absorption band at 1.69 eV and a peak that is located at 1.68 eV from the Koopmans ionization peak were identified incorrectly as arising from the same b_{3g} excited state. The b_{3g} excited state only gives rise to a satellite photoelectron peak, and hence, the 1.68-eV photoelectron peak is more suitably assigned to the transition to the b_{1u} excited state. The assignment of the 1.69-eV electronic absorption band is unchanged.

TABLE 4: Vertical Excitation Energies (eV) and Oscillator Strengths of Aromatic Heterocyclic Radical Cations

state (transition)	calculation: excitation energy[b]	calculation: oscillator strength	experiment: PE[c]	experiment: electronic absorption[d]
(**49**) Dibenzofuran[a] (C_{2v}, a_2)				
b_2 ($\pi_0^* \leftarrow \pi_{-1}$)	0.05	0.000	0.25	
a_2 ($\pi_0^* \leftarrow \pi_{-2}$)	0.93	0.000	1.26	1.41
b_2 ($\pi_0^* \leftarrow \pi_{-3}$)	2.28	0.202	1.97	1.91
a_1 ($\pi_0^* \leftarrow \sigma_{-4}$)	2.58	*e*	3.12*	
(**50**) Carbazole (C_{2v}, b_2)				
a_2 ($\pi_0^* \leftarrow \pi_{-1}$)	0.28	0.000	0.39	
a_2 ($\pi_0^* \leftarrow \pi_{-2}$)	1.59	0.078	1.46	1.53
b_2 ($\pi_0^* \leftarrow \pi_{-3}$)	1.84	0.002	2.15	1.87
a_1 ($\pi_0^* \leftarrow \sigma_{-5}$)	3.11	0.000	3.19*	
(**51**) Dibenzothiophene[a] (C_{2v}, b_2)				
a_2 ($\pi_0^* \leftarrow \pi_{-1}$)	0.19	0.000	0.41	
a_2 ($\pi_0^* \leftarrow \pi_{-2}$)	1.64	0.121	1.33	1.33
b_2 ($\pi_0^* \leftarrow \pi_{-3}$)	1.70	0.001	2.03	
b_2 ($\pi_0^* \leftarrow \pi_{-4}$)	2.85	0.049	2.72	2.66
a_1 ($\pi_0^* \leftarrow \sigma_{-5}$)	2.89	0.000	3.45*	

[a] Tamm−Dancoff approximation is used in the TDDFT calculation. [b] The parenthesis designates a satellite transition as described at the beginning of section 3. [c] Photoelectron spectra; taken from Ruščić et al.[55] The asterisk represents an onset of σ ionization manifold. [d] Taken from Shida.[30] [e] Forbidden.

The radical cations of triphenylene (**25**) and coronene (**28**) have degenerate ground state at the D_{3h} and D_{6h} geometries, respectively, and will undergo Jahn−Teller distortion if the geometries are allowed to distort. The TDDFT vertical excitation energies calculated at the D_{3h} and D_{6h} geometries are in overall good agreement with the experimental data, despite noticeable splitting of the expected degeneracy of the ground and some excited states. The splitting occurs because of the nonphysical symmetry breaking of Kohn−Sham orbitals in the ground state, which also affects the description of the excited states. This is a consequence of attempting to describe an intrinsically multideterminantal wave function of an open-shell system by a single determinant. Compared to Hartree−Fock theory, Kohn−Sham DFT is known to be resistant to symmetry breaking.[77,78] This seems to apply equally well to the corresponding single excitation theories; the size of the splitting of degenerate states is suppressed to a minimum in the TDDFT results. For example, the discrepancy from the perfect degeneracy of the ground state is only 0.03 eV for the triphenylene radical cation and 0.01 eV for the coronene radical cation. The discrepancy from the perfect degeneracy can be viewed as a precursor to the Jahn−Teller distortion, and consequently, the calculated excitation energies resemble the measured positions of the electronic absorption bands.

4. Concluding Remarks

TDDFT predicts vertical excitation energies of open-shell PAHs to within 0.3 eV of the experimental data with oscillator strengths that are consistent with the measured electronic absorption spectra. It offers a well-balanced description of σ and π orbitals and is generally capable of locating the onset of

TABLE 5: Vertical Excitation Energies (eV) and Oscillator Strengths of Aromatic Hydrocarbon Radical Anions

	calculation		experiment		calculation		experiment
state (transition)	excitation energy	oscillator strength	electronic absorption[a]	state (transition)	excitation energy	oscillator strength	electronic absorption[a]
			(**2**) Tetracene (D_{2h}, b_{3g})				
a_g ($\sigma_1^* \leftarrow \pi_0$)	1.05	*c*		a_u ($\pi_0^* \leftarrow \pi_{-1}$)	1.71	0.008	1.69
b_{2u} ($\sigma_2^* \leftarrow \pi_0$)	1.08	0.001		b_{3u} ($\sigma_8^* \leftarrow \pi_0$)	1.95	*c*	
b_{3u} ($\sigma_4^* \leftarrow \pi_0$)	1.37	*c*		b_{2u} ($\sigma_9^* \leftarrow \pi_0$)	1.97	0.001	1.91
b_{1g} ($\sigma_5^* \leftarrow \pi_0$)	1.54	*c*		b_{1u} ($\pi_{11}^* \leftarrow \pi_0$)	2.25	0.000	
b_{2g} ($\pi_6^* \leftarrow \pi_0$)	1.59	*c*		b_{3g} ($\pi_{10}^* \leftarrow \pi_0$)	2.25	*c*	
b_{1u} ($\pi_3^* \leftarrow \pi_0$)	1.63	0.180	1.50	b_{1g} ($\sigma_{12}^* \leftarrow \pi_0$)	2.43	*c*	
a_g ($\sigma_7^* \leftarrow \pi_0$)	1.63	*c*		a_g ($\sigma_{13}^* \leftarrow \pi_0$)	2.55	*c*	
			(**3**) Pentacene (D_{2h}, b_{1u})				
b_{2g} ($\pi_0^* \leftarrow \pi_{-1}$)	1.25	0.008	1.06[b]	a_g ($\sigma_7^* \leftarrow \pi_0$)	1.95	0.000	
a_g ($\sigma_2^* \leftarrow \pi_0$)	1.41	0.001		b_{3u} ($\sigma_9^* \leftarrow \pi_0$)	2.20	*c*	
b_{2u} ($\sigma_3^* \leftarrow \pi_0$)	1.42	*c*		b_{1u} ($\pi_8^* \leftarrow \pi_0$)	2.21	*c*	
b_{3g} ($\pi_1^* \leftarrow \pi_0$)	1.47	0.241	1.40[b]	b_{2u} ($\sigma_{10}^* \leftarrow \pi_0$)	2.22	*c*	
b_{3u} ($\sigma_4^* \leftarrow \pi_0$)	1.73	*c*		a_u ($\pi_1^* \leftarrow \pi_{-1}$)	2.32	*c*	
a_u ($\pi_5^* \leftarrow \pi_0$)	1.80	*c*		b_{1u} ($\pi_{12}^* \leftarrow \pi_0$)	2.55	*c*	
b_{1g} ($\sigma_6^* \leftarrow \pi_0$)	1.84	*c*		b_{3g} ($\pi_{11}^* \leftarrow \pi_0$)	2.55	0.003	2.82[b]
			(**6**) Chrysene (C_s, a″)				
a′ ($\sigma_1^* \leftarrow \pi_0$)	0.31	0.000		a″ ($\pi_{11}^* \leftarrow \pi_0$)	1.62	0.041	1.39
a′ ($\sigma_3^* \leftarrow \pi_0$)	0.36	0.001		a′ ($\sigma_{12}^* \leftarrow \pi_0$)	1.75	0.000	
a″ ($\pi_2^* \leftarrow \pi_0$)	0.38	0.000		a′ ($\sigma_{13}^* \leftarrow \pi_0$)	1.90	0.000	
a′ ($\sigma_5^* \leftarrow \pi_0$)	0.60	0.000		a″ ($\pi_{14}^* \leftarrow \pi_0$)	2.21	0.030	1.82
a″ ($\pi_4^* \leftarrow \pi_0$)	0.75	0.052	0.79	a′ ($\sigma_{15}^* \leftarrow \pi_0$)	2.33	0.000	
a′ ($\sigma_6^* \leftarrow \pi_0$)	0.81	0.000		a′ ($\sigma_{16}^* \leftarrow \pi_0$)	2.40	0.001	
a′ ($\sigma_7^* \leftarrow \pi_0$)	0.86	0.000		a″ ($\pi_{17}^* \leftarrow \pi_0$)	2.57	0.000	
a′ ($\sigma_8^* \leftarrow \pi_0$)	1.21	0.000		a″ ($\pi_{18}^* \leftarrow \pi_0$)	2.59	0.026	2.58
a′ ($\sigma_9^* \leftarrow \pi_0$)	1.29	0.002	1.23	a″ ($\pi_{19}^* \leftarrow \pi_0$)	2.67	0.000	
a″ ($\pi_{10}^* \leftarrow \pi_0$)	1.53	0.000					
			(**26**) Perylene (D_{2h}, b_{2g})				
a_g ($\sigma_1^* \leftarrow \pi_0$)	0.98	*c*		b_{3g} ($\pi_9^* \leftarrow \pi_0$)	1.78	*c*	
b_{2u} ($\sigma_2^* \leftarrow \pi_0$)	1.10	*c*		b_{2u} ($\sigma_{10}^* \leftarrow \pi_0$)	1.87	*c*	
b_{3u} ($\sigma_3^* \leftarrow \pi_0$)	1.16	0.003	1.24	b_{3u} ($\sigma_{11}^* \leftarrow \pi_0$)	1.97	0.007	1.83
b_{1u} ($\pi_4^* \leftarrow \pi_0$)	1.26	0.004	1.39	a_u ($\pi_0^* \leftarrow \pi_{-1}$)	2.30	0.331	2.15
b_{1g} ($\sigma_5^* \leftarrow \pi_0$)	1.37	*c*		a_g ($\sigma_{12}^* \leftarrow \pi_0$)	2.38	*c*	
a_g ($\sigma_7^* \leftarrow \pi_0$)	1.54	*c*		b_{1g} ($\sigma_{13}^* \leftarrow \pi_0$)	2.52	*c*	
b_{1u} ($\pi_6^* \leftarrow \pi_0$)	1.59	0.036	1.48	b_{3g} ($\pi_{14}^* \leftarrow \pi_0$)	2.71	*c*	
a_u ($\pi_8^* \leftarrow \pi_0$)	1.70	0.009	1.70	b_{1u} ($\pi_{15}^* \leftarrow \pi_0$)	2.80	0.024	
			(**30**) Pyrene (D_{2h}, a_u)				
a_g ($\sigma_1^* \leftarrow \pi_0$)	0.43	*c*		b_{2g} ($\pi_9^* \leftarrow \pi_0$)	1.59	0.038	1.74
b_{2u} ($\sigma_2^* \leftarrow \pi_0$)	0.55	*c*		a_g ($\sigma_{11}^* \leftarrow \pi_0$)	2.07	*c*	
b_{3u} ($\sigma_3^* \leftarrow \pi_0$)	0.69	*c*		b_{1u} ($\pi_{12}^* \leftarrow \pi_0$)	2.18	*c*	
b_{1u} ($\pi_4^* \leftarrow \pi_0$)	0.78	*c*		b_{1g} ($\sigma_{13}^* \leftarrow \pi_0$)	2.23	0.004	
a_g ($\sigma_5^* \leftarrow \pi_0$)	0.94	*c*		a_g ($\sigma_{14}^* \leftarrow \pi_0$)	2.36	*c*	
b_{1g} ($\sigma_6^* \leftarrow \pi_0$)	1.03	0.002		b_{3g} ($\pi_{15}^* \leftarrow \pi_0$)	2.46	0.001	
b_{3g} ($\pi_7^* \leftarrow \pi_0$)	1.22	0.010	1.22	a_u ($\pi_{16}^* \leftarrow \pi_0$)	2.66	*c*	
b_{2u} ($\sigma_8^* \leftarrow \pi_0$)	1.46	*c*		b_{3g} ($\pi_{17}^* \leftarrow \pi_0$)	2.72	0.025	
b_{3u} ($\sigma_{10}^* \leftarrow \pi_0$)	1.50	*c*		b_{2g} ($\pi_0^* \leftarrow \pi_{-1}$)	2.80	0.109	2.52
			(**41**) Azulene (C_{2v}, b_1)				
a_1 ($\sigma_1^* \leftarrow \pi_0$)	0.47	0.000		a_1 ($\sigma_7^* \leftarrow \pi_0$)	1.74	0.002	1.45
a_1 ($\sigma_2^* \leftarrow \pi_0$)	0.71	0.004	0.93	b_2 ($\sigma_8^* \leftarrow \pi_0$)	1.91	*c*	
b_2 ($\sigma_3^* \leftarrow \pi_0$)	0.77	*c*		b_1 ($\pi_9^* \leftarrow \pi_0$)	2.44	0.003	2.38
a_2 ($\pi_4^* \leftarrow \pi_0$)	0.86	0.000		a_2 ($\pi_0^* \leftarrow \pi_{-1}$)	2.48	0.000	
a_1 ($\sigma_5^* \leftarrow \pi_0$)	1.17	0.003	1.13	a_1 ($\sigma_{10}^* \leftarrow \pi_0$)	2.54	0.001	
b_2 ($\sigma_6^* \leftarrow \pi_0$)	1.22	*c*		a_2 ($\pi_{11}^* \leftarrow \pi_0$)	2.83	0.056	2.82
			(**47**) Biphenylene (D_{2h}, b_{2g})				
a_g ($\sigma_1^* \leftarrow \pi_0$)	0.08	*c*		b_{2u} ($\sigma_8^* \leftarrow \pi_0$)	1.32	*c*	
b_{2u} ($\sigma_2^* \leftarrow \pi_0$)	0.17	*c*		b_{1g} ($\sigma_{10}^* \leftarrow \pi_0$)	1.84	*c*	
b_{1u} ($\pi_3^* \leftarrow \pi_0$)	0.40	0.000		b_{3g} ($\pi_{11}^* \leftarrow \pi_0$)	1.97	*c*	
b_{3u} ($\sigma_4^* \leftarrow \pi_0$)	0.41	0.001		a_u ($\pi_9^* \leftarrow \pi_0$)	2.02	0.138	2.01
b_{1g} ($\sigma_5^* \leftarrow \pi_0$)	0.63	*c*		b_{1u} ($\pi_{12}^* \leftarrow \pi_0$)	2.29	0.007	2.14
a_g ($\sigma_6^* \leftarrow \pi_0$)	0.73	*c*		b_{3g} ($\pi_{13}^* \leftarrow \pi_0$)	2.42	*c*	
b_{3u} ($\sigma_7^* \leftarrow \pi_0$)	1.21	0.004	0.89				

[a] Taken from Shida,[30] unless otherwise noted. [b] Taken from Shida and Iwata.[22] [c] Forbidden.

σ ionization manifolds in photoelectron spectra. Correspondingly, it exhibits uniform accuracy for the excited states of PAH radical ions in which the mixing of σ and π orbitals occurs, for example, those that are nonplanar or contain sp^3 carbons. This is a desirable characteristic shared by TDDFT and many-body Green's function theory but often missed by active-space-based semiempirical or ab initio methods. TDDFT is, therefore, suitable for the study of hydrogen abstraction or addition

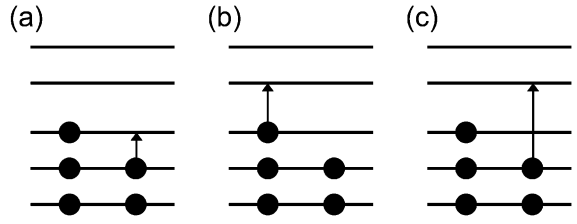

Figure 2. Diagrams of (a) Koopmans and (b and c) non-Koopmans states of radical cations.

reactions involving PAHs and perhaps the products of more complex photochemical reactions. Recent studies of fluorene, acenaphthylene, and acenaphthene by Szczepanski et al.[47−49] are prime examples.

TDDFT also maintains uniform accuracy between Koopmans and satellite transitions in photoelectron spectra. This may simply reflect the fact that TDDFT is an excited-state theory and it does not distinguish between these two types of transitions, in contrast to an ionization theory such as many-body Green's function theory, which treats them differently. The principal peaks in photoelectron spectra of neutral PAHs are assigned to the former type of transitions of the cations, whereas the latter types can often be seen, in addition to the former, in the electronic absorption spectra of the cations. TDDFT manifested its robustness to heterocyclic and nonbenzenoid rings. Rather unexpectedly, it has also been found that TDDFT can be used to interpret spectroscopic data of the PAH radical anions and even the slight spectral differences between cations and anions.

While it must be cautioned that this level of accuracy cannot always be achieved by TDDFT for any given molecule, TDDFT can be very useful for certain classes of molecules such as PAHs. The factors that make PAH radical cations and anions so well-suited for TDDFT may include the structural rigidity (so that geometric effects are relatively unimportant), the strong role of topology (adequate descriptions of orbitals by DFT for the ground states of radicals gives the leading picture of the lower excited states correctly), the unimportance of charge transfer effects (because of the uniform chemical composition), and the absence of Rydberg excited states. This study leads to the conclusion that the TDDFT approach is an excellent theoretical method for the study of the excited-state electronic structure, spectra, and photochemistry of PAHs and their derivatives, which appear increasingly important in many branches of chemistry.

Acknowledgment. The authors are indebted to Professor Suehiro Iwata (National Institution for Academic Degrees) for insightful discussions about the radical anions of PAH and to Dr. David A. Dixon (Pacific Northwest National Laboratory) for a critical reading of the manuscript prior to publication. The research performed at the William R. Wiley Environmental Molecular Sciences Laboratory (EMSL) at the Pacific Northwest National Laboratory (PNNL) was funded by the Office of Biological and Environmental Research in the U. S. Department of Energy. PNNL is operated by Battelle Memorial Institute for the U. S. Department of Energy under contract DE-AC06−76RLO 1830. S.H. and M.H.-G. acknowledge funding from the Director, Office of Basic Energy Sciences, Chemical Sciences Division of the U.S. Department of Energy. M.V. and J.S. gratefully acknowledge the donors of the Petroleum Research Foundation, administered by the American Chemical Society, and the National Aeronautics and Space Administration for their support of this research.

References and Notes

(1) Duley, W. W.; Williams, D. A. *Mon. Not. R. Astron. Soc.* **1981**, *196*, 269.
(2) Leger, A.; Puget, J. L. *Astron. Astrophys.* **1984**, *137*, L5.
(3) Allamandola, L. J.; Tielens, A. G. G. M.; Barker, J. R. *Astrophys. J.* **1985**, *290*, L25.
(4) van der Zwet, G. P.; Allamandola, L. J. *Astron. Astrophys*. **1985**, *146*, 76.
(5) Léger, A.; d'Hendecourt, L. *Astron. Astrophys.* **1985**, *146*, 81.
(6) Crawford, M. K.; Tielens, A. G. G. M.; Allamandola, L. J. *Astrophys. J.* **1985**, *293*, L45.
(7) Salama, F.; Allamandola, L. J. *Astrophys. J.* **1992**, *395*, 301.
(8) Frenklach, M.; Clary, D. W.; Gardiner, W. C.; Stein, S. E. *20th Symposium (International) on Combustion*; The Combustion Institute: Pittsburgh, PA, 1984; p 887.
(9) Bauer, S. H.; Jeffers, P. M. *Energy Fuels* **1988**, *2*, 446.
(10) Harris, S. J.; Weiner, A. M.; Blint, R. J. *Combust. Flame* **1988**, *72*, 91.
(11) Bjørseth, A.; Ramdahl, T. *Handbook of Polycyclic Aromatic Hydrocarbons*; Marcel Dekker: New York, 1983; Vol. 2, p 1.
(12) Harvey, R. G. *Polycyclic Aromatic Hydrocarbons*; Wiley-VCH: New York, 1996.
(13) Dabestani, R.; Ivanov, I. N. *Photochem. Photobiol*. **1999**, *70*, 10.
(14) Kroto, H. W.; Allaf, A. W.; Balm, S. P. *Chem. Rev.* **1991**, *91*, 1213.
(15) Curl, R. F. *Nature* **1993**, *363*, 14.
(16) Pope, C. J.; Marr, J. A.; Howard, J. B. *J. Phys. Chem.* **1993**, *97*, 11001.
(17) Szczepanski, J.; Vala, M. *Astrophys. J.* **1993**, *414*, 646.
(18) Szczepanski, J.; Vala, M. *Nature* **1993**, *363*, 699.
(19) Hudgins, D. M.; Sandford, S. A.; Allamandola, L. J. *J. Phys. Chem.* **1994**, *98*, 4243.
(20) Hudgins, D. M.; Allamandola, L. J. *J. Phys. Chem.* **1995**, *99*, 3033.
(21) Kim, H.-S.; Wagner, D. R.; Saykally, R. J. *Phys. Rev. Lett.* **2001**, *86*, 5691.
(22) Shida, T.; Iwata, S. *J. Am. Chem. Soc*. **1973**, *95*, 3473.
(23) Andrews, L.; Blankenship, T. A. *J. Am. Chem. Soc.* **1981**, *103*, 5977.
(24) Kelsall, B. J.; Andrews, L. *J. Chem. Phys.* **1982**, *76*, 5005.
(25) Andrews, L.; Kelsall, B. J.; Blankenship, T. A. *J. Phys. Chem.* **1982**, *86*, 2916 .
(26) Khan, Z. H. *Z. Naturforsch*. **1984**, *39a*, 668.
(27) Andrews, L.; Friedman, R. S.; Kelsall, B. J. *J. Phys. Chem.* **1985**, *89*, 4016.
(28) Khan, Z. H. *Z. Naturforsch.* **1987**, *42a*, 91.
(29) Khan, Z. H. *Spectrochim. Acta* **1988**, *44A*, 313.
(30) Shida, T. *Electronic Absorption Spectra of Radical Ions*; Physical Science Data 34; Elsevier: Amsterdam, 1988.
(31) Khan, Z. H. *Spectrochim. Acta* **1989**, *45A*, 253.
(32) Salama, F.; Allamandola, L. J. *J. Chem. Phys.* **1991**, *94*, 6964.
(33) Salama, F.; Allamandola, L. J. *J. Chem. Phys.* **1991**, *95*, 6190.
(34) Szczepanski, J.; Roser, D.; Personette, W.; Eyring, M.; Pellow, R.; Vala, M. *J. Phys. Chem.* **1992**, *96*, 7876.
(35) Szczepanski, J.; Chapo, C.; Vala, M. *Chem. Phys. Lett.* **1993**, *205*, 434.
(36) Khan, Z. H.; Husain, M. M.; Haselbach, E. *Appl. Spectrosc*. **1993**, *47*, 2140.
(37) Szczepanski, J.; Vala, M.; Talbi, D.; Parisel, O.; Ellinger, Y. *J. Chem. Phys.* **1993**, *98*, 4494.
(38) Salama, F.; Joblin, C.; Allamandola, L. J. *J. Chem. Phys.* **1994**, *101*, 10252.
(39) Vala, M.; Szczepanski, J.; Pauzat, F.; Parisel, O.; Talbi, D.; Ellinger, Y. *J. Phys. Chem.* **1994**, *98*, 9187.
(40) Joblin, C.; Salama, F.; Allamandola, L. J. *J. Chem. Phys.* **1995**, *102*, 9743.
(41) Szczepanski, J.; Wehlburg, C.; Vala, M. *Chem. Phys. Lett.* **1995**, *232*, 221.
(42) Szczepanski, J.; Drawdy, J.; Wehlburg, C.; Vala, M. *Chem. Phys. Lett.* **1995**, *245*, 539 .
(43) Salama, F.; Joblin, C.; Allamandola, L. J. *Planet. Space Sci.* **1995**, *43*, 1165.
(44) Bally, T.; Carra, C.; Fülscher, M. P.; Zhu, Z. *J. Chem. Soc., Perkin Trans.* **1998**, *2*, 1759.
(45) Halasinski, T. M.; Hudgins, D. M.; Salama, F.; Allamandola, L. J.; Bally, T. *J. Phys. Chem. A* **2000**, *104*, 7484.
(46) Ruiterkamp, R.; Halasinski, T.; Salama, F.; Foing, B. H.; Allamandola, L. J.; Schmidt, W.; Ehrenfreund, P. *Astron. Astrophys.* **2002**, *390*, 1153.
(47) Szczepanski, J.; Banisaukas, J.; Vala, M.; Hirata, S.; Bartlett, R. J.; Head-Gordon, M. *J. Phys. Chem. A* **2002**, *106*, 63.
(48) Szczepanski, J.; Banisaukas, J.; Vala, M.; Hirata, S. *J. Phys. Chem. A* **2002**, *106*, 6935.

(49) Banisaukas, J.; Szczepanski, J.; Eyler, J.; Vala, M.; Hirata, S.; Head-Gordon, M.; Oomens, J.; Meijer, G.; von Helden, G. *J. Phys. Chem. A* **2003**, *107*, 782.
(50) Boschi, R.; Schmidt, W. *Tetrahedron Lett.* **1972**, *25*, 2577.
(51) Boschi, R.; Murrell, J. N.; Schmidt, W. *Discuss. Faraday Soc.* **1972**, *54*, 116.
(52) Clark, P. A.; Brogli, F.; Heilbronner, E. *Helv. Chim. Acta* **1972**, *55*, 1415.
(53) Boschi, R.; Clar, E.; Schmidt, W. *J. Chem. Phys.* **1974**, *60*, 4406.
(54) Schmidt, W. *J. Chem. Phys.* **1977**, *66*, 828.
(55) Ruščić, B.; Kovač, B.; Klasinc, L.; Güsten, H. *Z. Naturforsch.* **1978**, *33a*, 1006.
(56) Niederalt, C.; Grimme, S.; Peyerimhoff, S. D. *Chem. Phys. Lett.* **1995**, *245*, 455.
(57) Rubio, M.; Merchán, M.; Ortí, E.; Roos, B. O. *J. Phys. Chem.* **1995**, *99*, 14980.
(58) Roos, B. O.; Andersson, K.; Fülscher, M. P.; Malmqvist, P.-Å.; Serrano-Andrés, L.; Pierloot, K.; Merchán, M. *Adv. Chem. Phys.* **1996**, *93*, 219.
(59) Deleuze, M. S.; Trofimov, A. B.; Cederbaum, L. S. *J. Chem. Phys.* **2001**, *115*, 5859.
(60) Deleuze, M. S. *J. Chem. Phys.* **2002**, *116*, 7012.
(61) Runge, E.; Gross, E. K. U. *Phys. Rev. Lett.* **1984**, *52*, 997.
(62) Gross, E. K. U.; Kohn, W. *Adv. Quantum Chem.* **1990**, *21*, 255.
(63) Casida, M. E. In *Recent Advances in Density Functional Methods*; Chong, D. P., Ed.; World Scientific: Singapore, 1995; Part I, p 155.
(64) Petersilka, M.; Gossmann, U. J.; Gross, E. K. U. *Phys. Rev. Lett.* **1996**, *76*, 1212.
(65) Bauernschmitt, R.; Ahlrichs, R. *Chem. Phys. Lett.* **1996**, *256*, 454.
(66) Jamorski, C.; Casida, M. E.; Salahub, D. R. *J. Chem. Phys.* **1996**, *104*, 5134.
(67) Hirata, S.; Lee, T. J.; Head-Gordon, M. *J. Chem. Phys.* **1999**, *111*, 8904.
(68) Weisman, J. L.; Lee, T. J.; Head-Gordon, M. *Spectrochim. Acta A* **2001**, *57*, 931.
(69) Hirata, S.; Head-Gordon, M. *Chem. Phys. Lett.* **1999**, *302*, 375.
(70) Maurice, D.; Head-Gordon, M. *J. Phys. Chem.* **1996**, *100*, 6131.
(71) Hirata, S.; Head-Gordon, M. *Chem. Phys. Lett.* **1999**, *314*, 291.
(72) *NWChem, A Computational Chemistry Package for Parallel Computers, A Development Version*; Pacific Northwest National Laboratory: Richland, WA, 2002.
(73) Casida, M. E.; Jamorski, C.; Casida, K. C.; Salahub, D. R. *J. Chem. Phys.* **1998**, *108*, 4439.
(74) Tozer, D. J.; Handy, N. C. *J. Chem. Phys.* **1998**, *109*, 10180.
(75) Coulson, C. A.; Rushbrooke, G. S. *Proc. Cambridge Philos. Soc.* **1940**, *36*, 193.
(76) Angliker, H.; Gerson, F.; Lopez, J.; Wirz, J. *Chem. Phys. Lett.* **1981**, *81*, 242.
(77) Bauernschmitt, R.; Ahlrichs, R. *J. Chem. Phys.* **1996**, *104*, 9047.
(78) Sherrill, C. D.; Lee, M. S.; Head-Gordon, M. *Chem. Phys. Lett.* **1999**, *302*, 425.